

See discussions, stats, and author profiles for this publication at: <https://www.researchgate.net/publication/347372848>

Feature-based Classification for Image Segmentation in Automotive Radar Based on Statistical Distribution Analysis

Conference Paper · September 2020

DOI: 10.1109/RadarConf2043947.2020.9266596

CITATIONS

3

READS

72

3 authors, including:



Yang Xiao

University of Birmingham

5 PUBLICATIONS 54 CITATIONS

[SEE PROFILE](#)



Marina Gashinova

University of Birmingham

217 PUBLICATIONS 2,345 CITATIONS

[SEE PROFILE](#)

Feature-based Classification for Image Segmentation in Automotive Radar Based on Statistical Distribution Analysis

Yang Xiao, Liam Daniel, Marina Gashinova

Microwave Integrated Systems Laboratory (MISL), University of Birmingham, UK

YXX752@student.bham.ac.uk

Abstract—Segmentation and potential classification of surface and obstacle regions in automotive radar imagery is the key enabler of effective path planning in autonomous driving. As opposed to traditional radar processing where clutter is considered as an unwanted return and should be effectively removed, autonomous driving requires full scene assessment, where clutter carries necessary information for situational awareness of the autonomous platform and needs to be fully assessed to find the passable areas. In this paper, the statistical distribution features of the radar intensity data of several road-related scenes including asphalt, grass, shadow and target object areas are investigated. The algorithm of classification is developed based on distribution feature extraction and a multivariate Gaussian distribution (MGD) model. Under test dataset recorded by multi-sensor suit was used to evaluate the confusion matrix and F1 score of this classification algorithm.

Keywords—*Automotive sensor, radar imaging, surface classification, statistical distribution feature extraction, multivariate Gaussian distribution, image segmentation.*

I. INTRODUCTION

Automotive sensors are the backbone of advanced driver assistant systems (ADASs) and sensing systems for self-driving cars since they can provide robust assessment of the proximate environment (up to several hundred meters) for path planning and decision making [1, 2]. As opposed to traditional ADAS systems, for autonomous driving the identification of passable areas is the key task to achieve the functionalities of autonomous path planning and obstacle avoidance [3]. One of the approaches to identify the passable region from the sensed data is to segment and classify the surfaces and objects viewed by various sensors within a scene.

Compared with electro-optical automotive sensor technologies such as LIDAR and camera, radar sensors have the advantage of reliability in adverse weather and lighting environment [4]. Conventional automotive radar is responsible for detecting the position and estimating the speed of objects, though it could potentially also provide wider scene information e.g. class of surface. Image segmentation and object classification have been investigated in remote sensing area [5], but have never been applied for automotive imaging radar. Traditional automotive radar does not possess the capabilities to effectively assess and classify clutter areas due to low resolution and low sensitivity to surface texture. The move into the Low-THz frequency region allows both resolution and high sensitivity to be achieved, therefore enabling high-resolution radar imagery [6], which can now be a subject of the classification based on the contours and characteristics of returns of imaged objects. The distribution features of

radar clutter coming from different surfaces which depends on the back scattering properties of those surfaces [7, 8], could provide the information for their classification. Then to achieve path planning using radar sensor images, segmentation and labelling of the different surfaces and obstacle areas within the radar imagery is required.

In this paper we consider the problem of classification of different areas within radar image maps as the main step for further image segmentation. The classification algorithm proposed is based on the statistical distribution parameters of radar intensity values received from different surfaces and obstacle regions. These are then used as feature parameters in a multivariate Gaussian distribution (MGD) model. The fitted parameters of five distributions, which are generally used for modelling radar clutter in the field of Synthetic Aperture Radar (SAR), are investigated using our gathered automotive radar image dataset. Confusion matrix results for different combinations of input distribution features are investigated to determine the proper input feature vector which could provide the best classification performance. Our supervised classification algorithm could provide the F1 score of 0.89, 0.96, 0.8 and 0.89 on asphalt, grass, shadow and target areas respectively.

II. AUTOMOTIVE RADAR IMAGE DATA SET

The automotive radar image dataset used in this paper is composed of radar intensity data and the optical images. The ground truth optical image is provided by a stereo video camera and used for initial manual labelling of the regions in the radar images.

A. Raw radar data

The measurement sensing system used in this paper comprises an experimental high resolution 79 GHz frequency modulated continuous waveform (FMCW) automotive radar designed by University of Birmingham and manufactured by ELVA-1 [9, 10], and the camera sensor. The automotive radar images are radar maps formed by augmented radar intensity range profiles obtained with 1.3° azimuth resolution in the scanned field of View (FoV) $\pm 45^\circ$ from boresight. A sequence of continuous maps (hereafter - frames) recorded from a moving car is combined to form a radar movie with the frame rate of 1 Hz. The dataset used in this paper was equally split into training and testing datasets. Fig. 1 (a) and (c) show the example of one radar image frame and the corresponding optical image. The data were recorded within the urban environment of the campus of the University of Birmingham, UK, which mainly contains asphalt roads, grass lawn areas along the road, a number of roadside related objects such as buildings, pedestrians, signposts and vehicles. Radar shadows behind such objects are of our particular interest, as their

identification within the radar imagery can potentially enhance classification of different obstacles using a context-based approach, and shadow depth could help to evaluate their height. For path planning, one of the generic approaches is to find only the regions which can be cleared by the vehicle and additionally to find regions of different road surfaces to (i) enable vehicle smooth transition between different road surfaces for example tarmac to grass area; (ii) identify the road edges by determining the boundaries between surfaces. Therefore, in this paper the 4 classes of areas for segmentation chosen are: asphalt/tarmac, grass, shadow and objects.

B. Automotive radar image labeling

All the radar images are labelled using the labelling tool of Liblable [11, 12], the tool operates on a raster image of the radar scan, not the raw range-azimuth data, corresponding video imagery guides the labelling. The labelled image of the radar frame in Fig. 1 (a) is shown in Fig. 1 (b), where the RGB pixels of the radar image belong to a specific class are marked out by the same color. The colors of asphalt, grass, shadow and target regions are green, blue, red and dark purple, respectively.

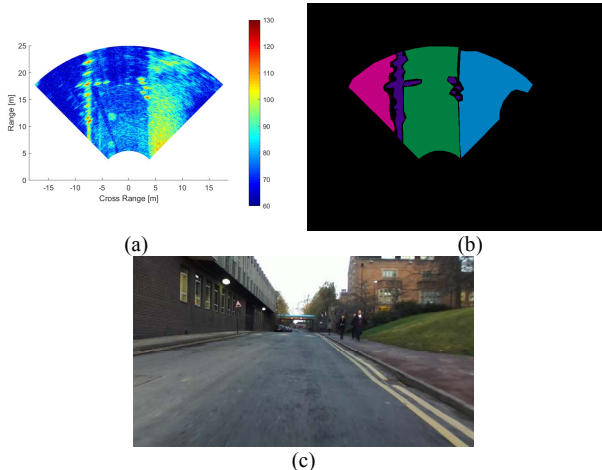


Fig. 1 Example of one frame of radar image data. (a) Radar image produced by radar intensity values; (b) Labelled image; (c) Optical image.

The pixels of areas which could not be associated with one of four classes in the optical image due to restricted visibility/uncertainty are discarded and shown as black background in the labelled image, though can be treated as belonging to the class “unknown”, which can be then refined in advanced context-based and associations approaches. The radar images present the detailed clutter map of the detected scene, where finally segments will be represented as areas with similar statistical characteristics of radar returns, such as type and kind of distribution and the distribution parameters. The radar intensity characteristics are estimated within similar labelled areas. The distribution features of radar clutter of different areas are explored based on the probability density histogram plot of radar intensity values.

III. STATISTICAL DISTRIBUTION FEATURE EXTRACTION

In this section, the distribution features of intensity values obtained from various region types are investigated by using following analysis steps: i) fitting histograms with known PDFs to find distribution parameters; ii) estimating

fitting errors of each distribution; iii) devising the distinguishable features of the distribution parameters between classes.

A. Method to extract distribution features

In the analysis of distribution features of radar intensity data, we use the FITTER [13] package which could effectively provide the fit results of 80 distribution types, including the fitting errors and the distribution parameters. We found that five bell-shaped PDFs - Weibull, normal, gamma, log-normal and log-gamma fit the histograms well. Therefore, this discussion is based on these five distributions. The definition of the PDFs and parameters of these distributions could be found in [14], we only show the definitions of distribution parameters here to simplify the further discussion of these parameters: 1) Weibull: shape parameter k and scale parameter λ ; 2) normal: mean μ and standard deviation σ ; 3) Gamma, lognormal and loggamma: shape parameter k , scale parameter λ and local parameter c .

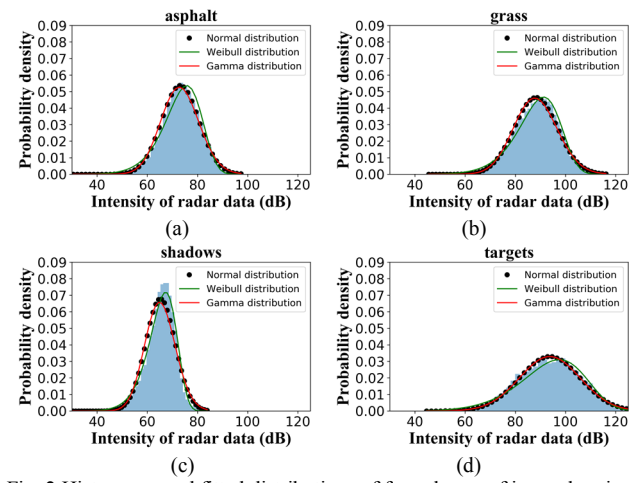


Fig. 2 Histograms and fitted distributions of four classes of imaged regions. Blue bars represent the histogram. The scale ranges of x-axis are the same for each inset. (a) results of asphalt; (b) results of grass; (c) results of shadows; (d) results of targets.

The histograms of radar intensity of asphalt, grass, shadows and targets areas and the fitted PDFs of distributions of Weibull, normal and Gamma are shown in Fig. 2. Since the PDFs of lognormal and loggamma are very similar to those of normal and Gamma, only results of three distributions are shown here. The radar intensities on the x-axis are not calibrated to any reference target, the scale is therefore arbitrary but consistent through all imagery recorded by the radar.

The histogram of intensities from areas containing target return demonstrate a wide spread in intensity and evidence of bimodality. However, for the purposes of showing that classes have distinctive differences, we fit unimodal distributions for all classes. Even though knowledge of the true distributions is essential for understanding of the underlying physical processes of the scattering, for the purposes of segmentation we only seek to find unique statistical descriptors that allow separation of the classes.

Let's stress here, that shadow area has the smallest variation range of radar intensities comparing to other classes since there are no signal returns and the intensity is mostly defined by the electronic noise of radar transceiver.

Comparison of the histograms in Fig. 2 (a) and (b) shows that grass area returns follow a slightly wider bell shape distribution than that of asphalt, which can be explained by wider deviations in the height profile of grass.

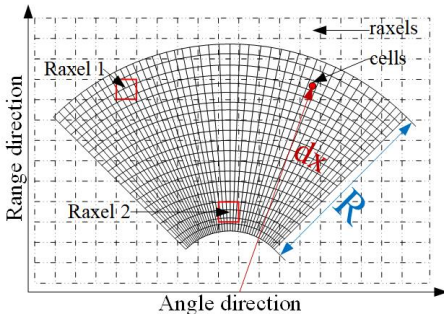


Fig. 3 Relationship between rixels of radar images and radar data cells.

As shown in Fig. 3, the extraction process of radar intensity values is based on two forms of the data. The radar range-azimuth map pixels (defined as “cells” here) plotted in Cartesian coordinates and the radar raster image pixels with three color channels (defined as “rixels” here). The task is to map the regions in the raster image to the appropriate cell intensities in the radar map. The azimuth dimension of each cell depends on their range. Therefore, rixels of the labeled image at different ranges correspond to a different number of cells of different azimuth resolution, e.g. raxel 1 and raxel 2 shown in Fig. 3. The relationship between the size of rixels and the sizes of cells is calculated in the following way. The resolution of cells is constant in range direction. Assume the number of cells is c_{nr} and the number of rixels is r_{nr} in the range direction, which both correspond to the range difference of R . One raxel corresponds to the number of $\lceil c_{nr}/r_{nr} \rceil$ of cells in range direction. In the azimuth direction, the relationship between the sizes of rixels and cells is a function related to the distance d_x . Assume the number of cells in the azimuth direction is c_{na} which corresponds to the angle range of A° . The number of cells corresponds to one raxel in angle direction can be denoted as $\lceil \frac{c_{na}R}{2AC_{nr}d_x\sin(0.5^\circ)} \rceil$. In our data set, the practical values of above parameters are: $c_{nr} = 668$, $r_{nr} = 308$, $R=20m$, $c_{na} = 199$ and $A = 90^\circ$. Therefore, one raxel corresponds to 3×2 cells in the range of 5m and 3×1 cells in the range of 25m. We took 3×2 cells from one raxel for all ranges to simplify the calculation and guarantee all intensities of the ROI are extracted. Each class of area in the labeled image has a different number of rixels therefore different number of cells of different sizes combined in the area super pixel. All the coordinates of cells are obtained based on the above mapping relationship between cells and rixels firstly. The coordinates of cells obtained are then examined in order to delete the repeat cells and extract the meaningful intensities for fitting distributions.

Due to propagation effects, the radar intensity level depends on the range to the cell. Additionally, clutter RCS depends on grazing angle, which reduces with range, therefore it is expedient to subdivide intensity values from cells into range groups, where we could assume consistency of statistical characteristics for each class to facilitate classification. The radar image covers ranges of 5–25m, with a radar height of 1 m the grazing angle across the imaged area varies from 11° to 2.3° at ranges of 5 and 25 m

respectively and 4 range groups are considered in this paper: 5–10m, 10–15m, 15–20m and 20–25m. The intensities extracted from one class of area is initially segmented into four range groups. Intensity values in each range group are further divided into radar data arrays of size 1000 to produce the histogram plot. The number of intensity values used for plotting each histogram is therefore identical. Computationally all described processing steps can be done in real time.

B. Analysis of the distribution features

Next the properties of the fitted distributions are analyzed based on the whole data set. To evaluate the fit errors of distributions and find out the distribution which best fits the radar intensity values of each considered class, the errors of distributions are shown in Fig. 4. The fitting error is estimated as:

$$\text{Error} = \sum_i (H_i - P_i)^2 \quad (1),$$

where H_i is the histogram value, P_i is the corresponded PDF values. The solid circle markers and the error bars in Fig. 4 represent the average error value and the standard deviation, respectively, these are calculated using the fit errors obtained from the whole data set.

We could observe from this result that Weibull and normal show smaller error and standard deviation than other distributions. The Weibull distribution is the distribution best fitted to the radar intensity values of all the four area types under study. The fitted distribution parameters of four distributions which could provide proper classification information are summarized for the different range regions in Fig. 5. In the results presented the solid marker shows the mean values of all the parameters in each range region while the error bar shows corresponding standard deviation of values.

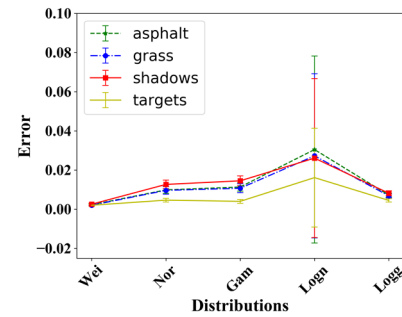


Fig. 4 Mean values and standard deviations of fitted errors of four areas under study for different distributions.

Let us discuss the distribution parameters separately. When comparing the 2-parameter distributions shown in Fig. 5 (a) and (b), the scale parameter (λ) of Weibull distribution and mean (μ) of Normal distribution show similar trend in the results for the four areas under study. These parameters reflect the intensity levels of the return signals from different ranges and this explains the decreasing behavior with the range. The slope of decrease for shadow areas is flatter than that for other areas since ‘signal’ in such areas mostly correspond to the noise of the radar system and in the ideal case will be independent of range. In reality, due to diffraction you may expect some scattering returns even from within the shadow regions. Target areas have the highest returns due to typically higher RCS than surfaces. Grass areas show higher reflected

intensity than asphalt due to the stronger back scattering caused by the rougher surface. These two parameters could provide significant information for further classification procedure since wide gaps and small overlaps between parameter results of different areas are observed.

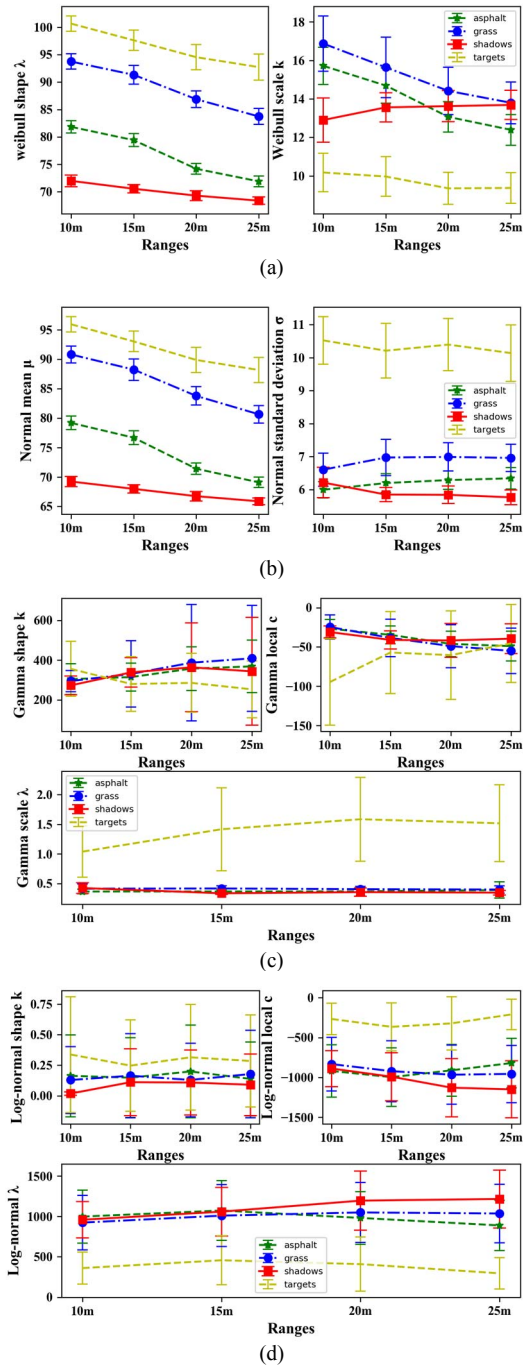


Fig. 5 Fitting parameters of Weibull (a), normal (b), gamma (c) and lognormal (d) distributions.

The scale parameter (k) of Weibull distribution and the standard deviation parameter (σ) of normal distribution could describe the bell shape of PDFs. Logically parameters of fits to areas with targets differ more from other classes because of the wider expected range of intensity values in the density histogram as observed in Fig. 2. No obvious trend is observed in these parameters over ranges. Importantly there is a significant difference in trends of shape factors for shadows, which indicate a potential for

confident recognition of shadow areas. Importance of shadow recognition for path planning is difficult to overestimate, as shadow indicate presence of the obstacle on the ground and allows evaluation of its position, height and extent, which can be used for the context-based recognition of road actors.

The areas of asphalt and shadows show similar properties in longer distance region, which can be explained as the comparatively low roughness of asphalt gives small returns at lower grazing angles, and the signal becomes comparable with the noise. The increase of radar frequency and thus the electromagnetic roughness of asphalt could improve this. Therefore at current operational frequency region this might result in higher confusion, though here as well context based analysis can improve results. As for the 3-parameter distributions shown in Fig. 5 (c) and (d), the main potential advantage for higher accuracy of classification can be seen only for target areas, which differ significantly from other classes reflected by behavior of k and λ parameters of log-normal and λ parameter of gamma. However big variation and overlaps in the results of asphalt, grass and shadows areas might result in higher confusion errors in the following classification procedure.

IV. CLASSIFICATION BASED ON DISTRIBUTION FEASTURE PARAMETERS

The discussion above showed that difference in feature parameters can be used for the classification between four area types. Our goal is to find out a method which could combine the contributions from these features in order to provide optimal classification for these four considered classes at least. Here we will consider use of the MGD model for classification, which could involve all the distribution feature parameters together as the input, while the output p value represents the probability of the under test ROI area belongs to one of the classes. The recall, precision and F1 score of classification of different combinations of input distribution parameters have been compared to find the best input feature combination. Confusion matrix results of the classification between asphalt, grass, shadow and targets areas will be given to demonstrate the performance of our classification algorithm.

A. Classification algorithm based on MGD

The distribution feature parameters used in this classification algorithm could be approximately described by normal distribution. MGD is the generalization of the one-dimensional normal distribution to higher dimensions which is widely used in the anomaly detection for unsupervised learning [15, 16]. The definition of the PDF of MGD is:

$$p(X_t) = \frac{1}{(2\pi)^{\frac{n}{2}} |\Sigma|^{\frac{1}{2}}} e^{-\frac{1}{2}(X_t - \mu)^T \Sigma^{-1} (X_t - \mu)} \quad (2),$$

Here, X_t is the input variable of the feature parameters which will be introduced later. The mean value array $\mu = [\mu_1, \mu_2, \dots, \mu_n]$ and the covariance matrix Σ are calculated using the distribution parameters obtained from training data, which is a 2-dimensinal matrix determined as $X_{train} = [x_1, x_2, \dots, x_n]$. X_{train} is in the size of $m \times n$. The width n represents the number of feature parameters

involved in the MGD model for classification. For example, when using the parameters of Weibull and normal distributions in our classification model, the training distribution parameter matrix can be represented as $X_{train} = [W_\lambda, W_k, N_\mu, N_\sigma]$ i.e. with $n = 4$. The length m depends on the number of training examples used for establishing the MGD model. Thus, each entry $x_i = [x_i^{(1)}, x_i^{(2)}, x_i^{(3)}, \dots, x_i^{(m)}]$ in X_{train} is an array of one specific feature parameter which is obtained from m groups of training intensity values. After extracting the training feature parameters X_{train} , the elements of array μ are defined as:

$$\mu_i = \frac{1}{m} \sum_{j=1}^m x_i^{(j)} \quad (3).$$

The covariance matrix Σ is of the size $n \times n$ and defined as:

$$\Sigma = \frac{1}{m} \sum_{j=1}^m (x_i^{(j)} - \mu_i)(x_i^{(j)} - \mu_i)^T \quad (4).$$

Four groups of training feature parameters are extracted from four classes of areas of training data and presented as $(X_{train}^{asphalt}, X_{train}^{grass}, X_{train}^{shadow}, X_{train}^{target})$. Therefore, the MGD based classification of the four areas under study is developed by calculating the covariance matrix Σ and μ array of each of the four classes of areas. The covariance matrix Σ and the mean array μ of areas of asphalt, grass, shadows and targets can be represented as $[\Sigma_a, \Sigma_g, \Sigma_s, \Sigma_t]$ and $[\mu_a, \mu_g, \mu_s, \mu_t]$. Therefore, the MGD model is denoted as:

$$p(X_t) = [p_a(X_t, \Sigma_a, \mu_a), p_g(X_t, \Sigma_g, \mu_g), \\ p_s(X_t, \Sigma_s, \mu_s), p_t(X_t, \Sigma_t, \mu_t)] \quad (5).$$

We also considered the range gating in the feature extraction and classification procedure as discussed in section III.B. Four range-related sub-groups are used when evaluating the feature parameters of training data. Therefore, the covariance matrix and mean array are also generated for four range groups.

Let's consider as example, the characterization of the asphalt class. The classification probability $p_a(X_t, \Sigma_a, \mu_a)$ for radar intensity data which belongs to one of four range related groups will be either of 4 entities in:

$$p_a(X_t, \Sigma_a, \mu_a) = [p_{a1}(X_t^{r1}, \Sigma_a^{r1}, \mu_a^{r1}), p_{a2}(X_t^{r2}, \Sigma_a^{r2}, \mu_a^{r2}), \\ p_{a3}(X_t^{r3}, \Sigma_a^{r3}, \mu_a^{r3}), p_{a4}(X_t^{r4}, \Sigma_a^{r4}, \mu_a^{r4})] \quad (6).$$

The input feature array $X_t = [x_{t1}, x_{t2}, \dots, x_{tn}]$ is obtained from a non-classified ROI in the test data set, which is a 1-dimensional distribution parameters array in the size of $1 \times n$. Entries x_{ti} represents the feature parameters which correspond to similar parameters x_i in X_{train} . When inputting X_t into the MGD function of each area class, if X_t is within range group of r_i , then MGD model $p_{ai}(X_t^{ri}, \Sigma_a^{ri}, \mu_a^{ri})$ will be used for the calculation of p_a . The calculated p_a value represents the distribution feature similarity between the area under-test and an asphalt area. In every test, four p values are obtained by calculating the MGD function of four areas as in Eq. (5), which are represented as $[p_a, p_g, p_s, p_t]$. The under test area is classified as the type (a,g,s, t) corresponding to the largest p value.

B. Confusion matrices of the classification between four areas

When estimating the classification performance, a number of test feature arrays are extracted from the test data set using the method introduced above in section III. The under test feature arrays are classified using our classification algorithm and then compared with their manually labelled area class. The performance of the proposed classification procedure is estimated for three input combinations of distribution parameters: 1) All feature parameters of five distributions; 2) Four parameters of Weibull and normal distributions; 3) The shape and scale parameters of Weibull distribution. In case 1, the obtained F1 score is worse than the other cases. This can be explained as the overfitting phenomenon caused by the redundant features which could not provide useful information to classification. The input features of case 2 and 3 give the best classification performance, and the confusion matrix results of these two cases are shown in Table 1 and 2 below. F1 scores are calculated and used for estimating the classification performance which could help seek a balance between precision and recall of classification [17]. Results of recall, precision and F1 score are shown in the confusion matrices as well.

TABLE 1. CONFUSION MATRIX WHEN INPUT FEATURE IS COMBINED OF WEIBULL AND NORMAL DISTAIBUTION PARAMETERS

		Actual			
		Asphalt	Grass	Shadows	Targets
Predicted	Asphalt	725	0	104	0
	Grass	6	747	1	18
	Shadows	65	0	367	0
	Targets	3	41	0	262
Recall		0.91	0.95	0.78	0.94
Precision		0.8	0.97	0.85	0.86
F1 score		0.89	0.96	0.8	0.89

TABLE 2. CONFUSION MATRIX WHEN INPUT FEATURE OBTAINED FROM WEIBULL DISTRIBUTION PARAMATERS

		Actual			
		Asphalt	Grass	Shadows	Targets
Predicted	Asphalt	717	0	112	0
	Grass	18	755	0	23
	Shadows	64	0	360	0
	Targets	0	33	0	257
Recall		0.9	0.96	0.76	0.92
Precision		0.86	0.95	0.85	0.89
F1 score		0.88	0.95	0.8	0.9

The difference in classification results between case 2 and 3 is very small, yet, reduction of parameter extraction required by using only the Weibull distribution can be extremely beneficial for large amounts of test data. Therefore for the sake of reducing computing load segmentation can be based on this simplest case.

The classification based on the distribution features and the MGD model of asphalt, grass and target areas shows an F1 score of not less than 0.88 with grass being the best are

classified with an F1 score of higher than 0.95. Results shown here are based on analysis of 2339 test data arrays with 799 for asphalt, 788 for target areas, 472 for grass, and 280 for shadow areas. The F1 score of classification of shadow is less accurate, at about 0.8 due to the asphalt at longer distance and shadows areas have higher chance to be confused. The confusion between target areas and grass areas can be explained as two reasons: 1) The short bushes inside the grass area could not be totally omitted when labelling and have closer distribution properties to targets—in the future these may occupy their own class to attempt to remove confusion; 2) The raised lawn areas might be classified as targets—sloped and raised regions of surface have a differing grazing angle compared to ground level regions at the same range e.g. a sloped region of grass may be at a grazing angle similar to a nearer region of flat grass and display similar scattering characteristics but at a longer range—3D imagery would help to alleviate any confusion in surface orientation.

V. EXAMPLE SEGMENTATION RESULT

The proposed classification method can be used as a base for the important task of segmentation of radar images, which aims at informing path planning in autonomous driving. Methodology and results of the research on segmentation on radar images will be shown at the conference and presented in full-size journal publication which is currently in progress. For illustration only one example of segmentation in a single frame of radar imagery is shown in Fig. 6. The color coding is used for classified segments which are: asphalt (blue), grass (green), targets (yellow) and shadows (grey).

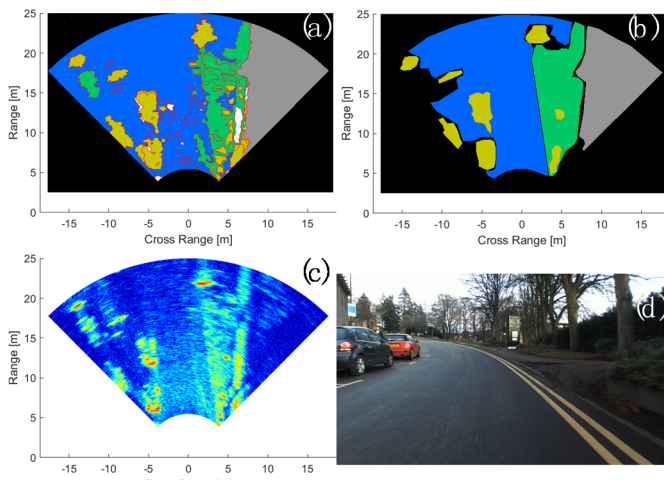


Fig. 6 The fully segmented radar image based on the supervised classification algorithm proposed in this paper. (a) The fully segmented radar image result; (b) The manual labelling image; (c) The radar image; (d) The optical image.

VI. CONCLUSION

In this paper, we explored the feasibility of classification of four classes of areas (asphalt, grass, shadows and targets areas) in high-resolution automotive radar imagery. The distribution features of four classes are analyzed based on distribution fits. Fit errors are estimated and Weibull distributions of varying parameters are found to be the best fit to each class in our collected radar data. Range-based pre-segmentation of areas to be classified is made to improve

classification which takes into account differences in statistical parameters of returns, which depend on the range/grazing angle. The distribution feature extraction identified differences between the four classes and thus the algorithm of classification based on the MGD model is then developed, confusion matrices are evaluated for the chosen classes of surfaces for different feature vectors. Using the combined features of Weibull and normal distributions as model inputs, or using the features of Weibull distribution alone provides good classification performance. The F1 score of asphalt, grass and targets are all higher than 0.88 and that of shadows is 0.8. The development of full segmentation algorithm for the radar imagery is ongoing and further results will be shown at the conference. Part of this ongoing work will investigate joint analysis of consecutive radar frames to aid in increasing confidence of classification, building on the single frame technique shown here.

REFERENCES

- [1] S. M. Patole, M. Torlak, D. Wang, and M. Ali, "Automotive radars: A review of signal processing techniques," *IEEE Signal Processing Magazine*, vol. 34, no. 2, pp. 22-35, 2017.
- [2] W. J. Fleming, "New automotive sensors—A review," *IEEE Sensors Journal*, vol. 8, no. 11, pp. 1900-1921, 2008.
- [3] L. Daniel, D. Phippen, E. Hoare, M. Cherniakov, and M. Gashinova, "Image Segmentation in Real Aperture Low-THz Radar Images," in *2019 20th International Radar Symposium (IRS)*, 2019, pp. 1-8: IEEE.
- [4] L. Daniel, D. Phippen, E. Hoare, A. Stove, M. Cherniakov, and M. Gashinova, "Low-THz radar, lidar and optical imaging through artificially generated fog," 2017.
- [5] M. D. Hossain, D. J. I. J. o. P. Chen, and R. Sensing, "Segmentation for Object-Based Image Analysis (OBIA): A review of algorithms and challenges from remote sensing perspective," vol. 150, pp. 115-134, 2019.
- [6] D. Jasteh, E. G. Hoare, M. Cherniakov, and M. Gashinova, "Experimental low-terahertz radar image analysis for automotive terrain sensing," *IEEE Geoscience and Remote Sensing Letters*, vol. 13, no. 4, pp. 490-494, 2016.
- [7] F. Galland, J.-M. Nicolas, H. Sportouche, M. Roche, F. Tupin, and P. Réfrégier, "Unsupervised synthetic aperture radar image segmentation using Fisher distributions," *IEEE Transactions on Geoscience and Remote Sensing*, vol. 47, no. 8, pp. 2966-2972, 2009.
- [8] E. E. Kuruoglu and J. Zerubia, "Modeling SAR images with a generalization of the Rayleigh distribution," *IEEE Transactions on Image Processing*, vol. 13, no. 4, pp. 527-533, 2004.
- [9] <http://elva-1.com/>.
- [10] Y. Xiao, F. Norouzian, E. G. Hoare, E. Marchetti, M. Gashinova, and M. J. I. S. J. Cherniakov, "Modelling and Experiment Verification of Transmissivity of Low-THz Radar Signal through Vehicle Infrastructure," 2020.
- [11] <http://www.cvlabs.net/software/liblabel/>.
- [12] A. Geiger, M. Lauer, C. Wojek, C. Stiller, R. J. I. t. o. p. a. Urtasun, and m. intelligence, "3d traffic scene understanding from movable platforms," vol. 36, no. 5, pp. 1012-1025, 2013.
- [13] <https://pypi.org/project/fitter/>.
- [14] <https://docs.scipy.org/doc/scipy/reference/stats.html>.
- [15] M. Goldstein and S. Uchida, "A comparative evaluation of unsupervised anomaly detection algorithms for multivariate data," *PloS one*, vol. 11, no. 4, p. e0152173, 2016.
- [16] G. G. Hazel, "Multivariate Gaussian MRF for multispectral scene segmentation and anomaly detection," *IEEE transactions on geoscience and remote sensing*, vol. 38, no. 3, pp. 1199-1211, 2000.
- [17] L. Zhong, L. Hu, and H. J. R. s. o. e. Zhou, "Deep learning based multi-temporal crop classification," vol. 221, pp. 430-443, 2019.